EUROMAT 2009

SiC/SiC and SiC/Kovar joining by Ni–Si and Mo interlayers

G. W. Liu · F. Valenza · M. L. Muolo ·
A. Passerone

Abstract A composite joining technique, using a Ni–56Si filler alloy and Mo as interlayers, was used to join SiC to SiC and to Kovar. The wetting of the Ni–Si alloy on SiC ceramic was studied in a vacuum at 1,350 °C by the sessile drop technique as a function of time; the non-reactive wetting characteristics in the Ni–Si/SiC system were confirmed, with an equilibrium contact angle of about 23°. SiC/SiC joints were fabricated by two processes using a Ni–Si/Mo/Ni–Si structure as the interlayer. SiC/Kovar joints were produced by means of a multilayer structure: molybdenum, which is used as the interlayer, was joined to Kovar on one side by means of transient liquid phase bonding and to SiC on the other side, using a Ni–Si coating as a filler alloy. The resulting joints were analyzed and discussed in terms of joint morphology and microstructure, joint strength, and fracture behavior. Two interfacial layers form at the Kovar/Mo and the Mo/Ni–Si interfaces due to dissolution and interdiffusion phenomena between the metallic elements, without there being any observable reactions with the SiC component. The type of joining process and the experimental conditions used play a key role in determining the joint microstructure and composition, the joint strength and its fracture behavior.

G. W. Liu · F. Valenza (✉) · M. L. Muolo · A. Passerone
Institute for Energetics and Interphases, IENI-CNR,
Via De Marini 6, 16149 Genoa, Italy
e-mail: valenza@ge.ieni.cnr.it

G. W. Liu
State Key Laboratory for Mechanical Behavior of Materials,
Xi'an Jiaotong University, 710049 Xi'an, China

Introduction

Silicon carbide is of great technological significance due to its good overall chemical, thermal, and mechanical properties, which make it a suitable candidate for aggressive environments. It is used as a both structural and functional material; indeed, it is currently used in high-temperature applications, such as metal–matrix composites, fusion reactors, heat exchangers, aerospace applications, etc. [1–3]. However, like most engineering ceramics, SiC is brittle and shows poor machinability, thus making it difficult to fabricate complex-shaped, large-sized components: joining ceramic to ceramic or to metals can overcome these drawbacks to a great extent.

At present, the techniques for joining SiC to itself or to metals for high-temperature applications include mainly brazing [4–9], diffusion bonding [10–14], and self-propagating high-temperature synthesis (SHS) welding [15, 16].

Liquid phase joining of ceramics, including the brazing process and the transient liquid phase bonding (TLPB) technique [17, 18], is promising because of its simplicity and high efficiency. Liquid phase joining of SiC can be obtained by reactive [4–9, 19] or non-reactive [20–23] joining processes. At the same time, studies on reactive [24–28] and non-reactive [29–33] wetting of metallic alloys on an SiC substrate were investigated. As excessive interfacial reactions between the filler metal and the SiC component are responsible for the formation of cracks, leading to the invalidation of the joint, many researchers have endeavored to look for some non- or low-reactive joining processes for SiC by using, for example, binary or ternary compounds with a high silicon content as brazing alloys [20–23, 34–36]. In addition, Hattali et al. [37] recently reported a non-reactive solid state bonding technique for joining SiC to nickel alloy via Ni and Ag interlayers.

The study presented here is a part of a program aimed at realizing effective SiC/SiC and SiC/Kovar joints using a composite joining technique, where Mo is used as an interlayer material due to its low thermal expansion coefficient (CTE $\sim 5 \times 10^{-6}$ °C^{-1} at 0–100 °C), close to that of the SiC (CTE $\sim 3 \times 10^{-6}$ °C^{-1} at 0–100 °C).

First of all, the wetting and interfacial behavior of Ni–56Si in contact with SiC, Mo, and Kovar were investigated and analyzed before starting the joining experiments. The results have already been reported [28] and are recalled briefly here.

Two processes for joining SiC to SiC using Ni–56Si (all compositions are given in at.% throughout the text) coatings and a Mo foil as interlayer are reported.

SiC/Kovar joints have interesting potential applications due to the good thermophysical properties of Kovar and the good CTE match (~ 4.6–5.2×10^{-6} °C^{-1} at 20–400 °C). They were produced using a multilayer structure: a molybdenum interlayer was joined to Kovar on one side using transient liquid phase bonding and to SiC on the other using a Ni–56Si coating as a filler alloy.

The resulting joints are discussed in terms of joint morphology and microstructure, joint strength, and fracture behavior.

Experimental process

Materials

A commercial Ni–56Si atomized powder (Goodfellow, England, size: 150 μm) was used. The Ni–Si alloy for wetting experiments was prepared by melting the commercial powder at 1,100 °C for 15 min under a vacuum of $\sim 3 \times 10^{-4}$ Pa.

The SiC pieces ($\varnothing 15$ mm $\times 2$ mm) used as substrate in wetting experiments were prepared by the hot isostatic pressing (HIP) process by adding 1% Al$_2$O$_3$ (vol.%) as a sintering aid, with a porosity of about 0.5% and a surface roughness, after polishing, of $R_a = 20$ nm. The SiC pieces ($\varnothing 15$ mm $\times 3$ mm) used in the joining experiments were fabricated by means of the plasma active sintering (PAS) technique by adding 6% Al$_2$O$_3$ and 4% Y$_2$O$_3$ (vol.%) as a sintering aid, the preparation process, composition, and properties of which are reported in the literature [38].

Pure Mo was used in the form of disks (diameter: 15 mm, thickness ~ 400 μm) or foil (Goodfellow, England, purity: 99.9%, thickness: 100 μm).

The nominal composition of the Kovar alloy, as reported by the suppliers and checked by energy dispersive spectroscopy analysis (EDS), is Fe–32Ni–15Co; this alloy was used in the form of disks with a diameter of 15 mm and a thickness of 3 mm.

Wetting and joining procedures

Before each wetting or joining experiment, all the substrates and components were given a final polishing and were carefully cleaned ultrasonically in alcohol. The Ni–Si alloy pieces for the wetting experiments were chemically and ultrasonically cleaned, and then dried. The wetting and spreading kinetics were evaluated by contact angle and drop dimensions measurements using the sessile drop technique in conjunction with the ad hoc designed ASTRAView image analysis software [39, 40]. Even if the software can calculate the contact angles with a precision of $\pm 0.5°$, possible optical distortions, due to the high temperature, can lead to uncertainties in the measured profiles [41], thus the contact angle values are given here with a precision of $\pm 2°$. Sessile drop tests were performed in an apparatus described in more detail in a recent article [42] at 1,350 °C under a vacuum of about 5×10^{-4} Pa.

For the joining experiments, a Ni–Si paste was prepared from a mixture of Ni–56Si alloy powder, diethyl oxalate, and collodion, with a preparation process similar to the one used for the preparation of TiH$_2$ paste [43].

SiC/SiC joints were produced by two joining process; in the first one (Process A), both sides of the Mo foil were painted first with the Ni–Si paste (thickness of the coating: ~ 50 μm), air-dried, pre-wetted in a vacuum of $\sim 3 \times 10^{-4}$ Pa at 1,200 °C for 5 min, and then cut into pieces measuring $\varnothing 15$ mm; finally the SiC/(Ni–Si)Mo (Ni–Si)/SiC multilayer samples were assembled and joined at 1,350 °C for 10, 30, or 50 min. In the second joining process (Process B), both sides of the Mo piece were painted with the Ni–Si paste and then air-dried; finally the SiC/(Ni–Si)Mo(Ni–Si)/SiC samples were directly assembled (without pre-wetting) and joined at 1,350, 1,375, or 1,400 °C for 10 min.

In order to evaluate the shear strength, some joints were cut into samples with dimensions of about 6 mm $\times$ 6 mm $\times$ 10 mm for shear tests which were conducted using the INSTRON 8501 mechanical testing machine in displacement control with a loading speed of 0.1 mm min^{-1}; the fixing system is specifically designed to allow the samples to be held with the interface exactly parallel to the direction of the load, which is applied along the interface (Fig. 6c).

In the Mo/Kovar joining process, the Mo ($\varnothing 15$ mm $\times$ 2 mm) and the Kovar ($\varnothing 15$ mm $\times$ 3 mm) discs were directly joined by means of a transient liquid phase bonding technique at 1,350 °C for 10 or 20 min. The phenomena occurring during the Mo/Kovar contact heating were further investigated by differential thermal analysis (DTA) technique using a Setaram Labsys apparatus with heating and cooling rates of 5 °C/min.

The SiC/Kovar joining process results from the combination of the previous techniques: one side of the Mo disk

was painted with a Ni–Si paste and air-dried. Then, the SiC/(Ni–Si)Mo/Kovar couple was assembled and joined at 1,350 °C for 10 min.

For all the joining processes, the heating rates were ~ 10 and 5 °C min^{-1} before and after 1,300 °C, respectively, and the cooling rate 5 °C min^{-1}, the samples were put in the furnace under a vacuum of 5×10^{-4} Pa. Each couple was mechanically charged (~ 1 kPa) in order to assure good contact between the layers.

The solidified sessile drop/substrate couple and joints were cross-sectioned, polished and observed by optical microscope and by scanning electron microscopy (SEM) coupled with EDS analysis.

Results and discussion

Wetting

The complete results on the wetting and spreading of SiC, Mo, and Kovar by Ni–Si as a function of temperature and atmosphere, are reported in [28]. It is worth recalling here that the spreading kinetics of the Ni–Si alloy on SiC at 1,350 °C in a vacuum measured according to the changes of drop dimensions (relative base diameter and drop height) and contact angle, reaches equilibrium nearly 400 s after melting, with a final contact angle of $\sim 23°$, a very good value for joining processes.

Figure 1 shows the SEM micrograph of the cross-sectioned Ni–Si/SiC interface, which is macroscopically smooth and sharp, without any precipitates and reaction products. Indeed, as explained by some authors by means of thermodynamic considerations and of the ternary Ni–Si–C
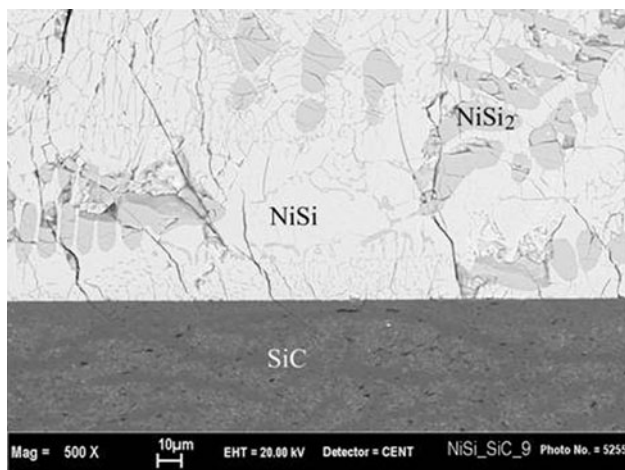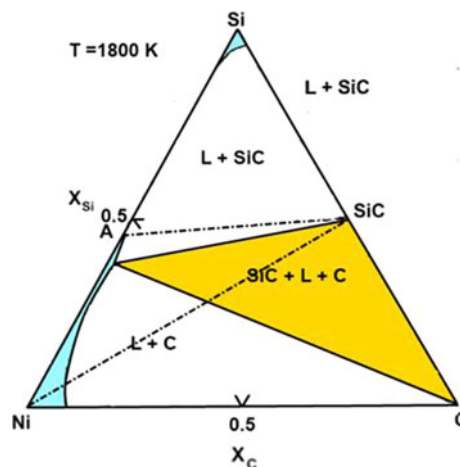

Fig. 2 Ni–Si–C phase diagram at 1,800 K (redrawn from [45])

diagram [44, 45], an equilibrium is established between the Ni–Si alloy and SiC when the original content of Si in Ni is above $\sim 40\%$, above 1,300 °C. As shown in Fig. 2, where the schematic Ni–Si–C phase diagram is shown at about 1,530 °C, when pure Ni comes into contact with SiC, a certain amount of Si dissolves into the liquid phase (with simultaneous precipitation of C), until its activity is in equilibrium with SiC. At about $X_{Si} = 0.4$, the saturated liquid alloy does not react with the solid substrate any more, leaving an undisturbed, flat interface. According to the EDS analysis, the two white and gray phases are NiSi and NiSi$_2$, respectively. Some cracks were found at the interface and in the bulk phases during cooling (samples were nearly quenched from test to room temperature) due to the presence of the brittle silicides (NiSi and NiSi$_2$) and to the thermal expansion coefficient difference between the Ni–Si alloy and the SiC.

SiC/SiC joining

The interface microstructures of cross-sectioned SiC/SiC joints, prepared by the two different joining processes, are shown in Fig. 3. The composition of the different phases in the joint interlayers, analyzed by dot mode, is listed in Table 1, while Fig. 4 shows the elemental EDS profiles across the SiC/Mo interface of a SiC/SiC joint.

As predicted by wetting experiments, the SiC/interlayer interfaces are very smooth and clean without visible reaction products or precipitates. A double-layer structure (layers A and B) forms at the Ni–Si/Mo interfaces. Two phases (dark-C and gray-D) exist in the Ni–Si layers of the joints fabricated at 1,350 °C for 10 min using the two joining processes, as shown in Fig. 3b, d. In addition, there are some holes in the position of the original Ni–Si coating, resulting from the degassing of the coating slurry during thermal cycling (Fig. 3). However, the zones C and D
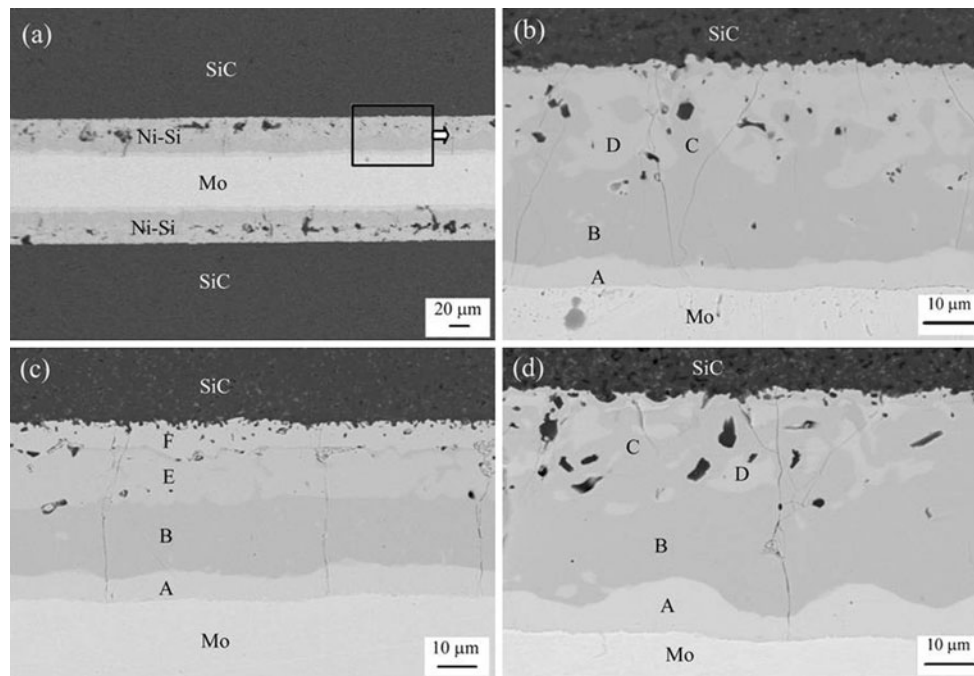

Fig. 1 Cross-section SEM micrograph (Back Scattered—BS mode) of the Ni–Si/SiC couple at 1,350 °C, showing the non-reactive wetting characteristics. The *white* and *gray* phases in the drop are NiSi and NiSi$_2$, respectively

Fig. 3 Interface SEM micrographs (BS mode) of cross-sectioned SiC/SiC joints: **a** and **b** 1,350 °C × 10 min, Process A; **c** 1,350 °C × 50 min, Process A; **d** 1,350 °C × 10 min, Process B, showing the microstructural evolution of the joint interlayers

Table 1 Compositions of characteristic microstructures of the joint interlayers shown in Fig. 3

Position	Composition (at.%)						Position	Composition (at.%)		
	1,350 °C × 10 min, Process A			1,350 °C × 10 min, Process B				1,350 °C × 50 min, Process A		
	Mo	Ni	Si	Mo	Ni	Si		Mo	Ni	Si
Layer A	63.9	1.6	34.5	63.4	1.5	35.1	Layer A	63.1	1.7	35.2
Layer B	37.1	30.6	32.3	36.9	29.6	33.4	Layer B	38.0	29.8	32.2
Phase C	35.1	33.3	31.6	35.8	32.8	31.4	Layer E	51.2	13.6	35.2
Phase D	51.1	13.6	35.3	49.7	14.2	36.1	Layer F	53.2	25.0	21.8

evolve gradually into two layers (E, which has the same composition of D, and F, which is rich in Mo) as the holding time is increased, as shown in Fig. 3c.

The microstructures and compositions of the SiC/SiC joints prepared by Process B (without pre-wetting) at three temperatures (1,350, 1,375, and 1,400 °C) are very similar to those of Fig. 3a, except for the size of the holes. Their size in Process A is finer due to the pre-wetting treatment.

As shown in Fig. 4 and Table 1, Ni is present mainly in the dark phases (in zone C and layer B); however, it can hardly be detected in the thin interfacial layer (layer A) near the Mo. So, the formation of the interfacial layer occurs mainly as a result of the interactions (diffusion and reaction) between Si and Mo. The Si contents are more or less equivalent (31–36%) in all the layers when using the holding time of 10 min. However, a 10% decrease is measured in layer F (near the ceramic) when using the longest holding time.

A SiC/SiC joint and two representative specimens prepared for shear tests are shown in Fig. 5. There are no visible interfacial reactions or macro-cracks in the interfacial region or within the samples. This shows that the joining process is quite effective. The shear strength of joints prepared by the two processes under different conditions is shown in Table 2. The joint shear strength values, directly calculated as $\sigma = P/A$ (where σ is the shear strength, P the shear load, and A the sectional area), are somewhat low due to the limited mechanical pressure applied to the samples during the process. The joint strength value decreases with increasing holding time when using Process A. Under the same conditions (1,350 °C × 10 min), the joint strength is higher when using Process B.
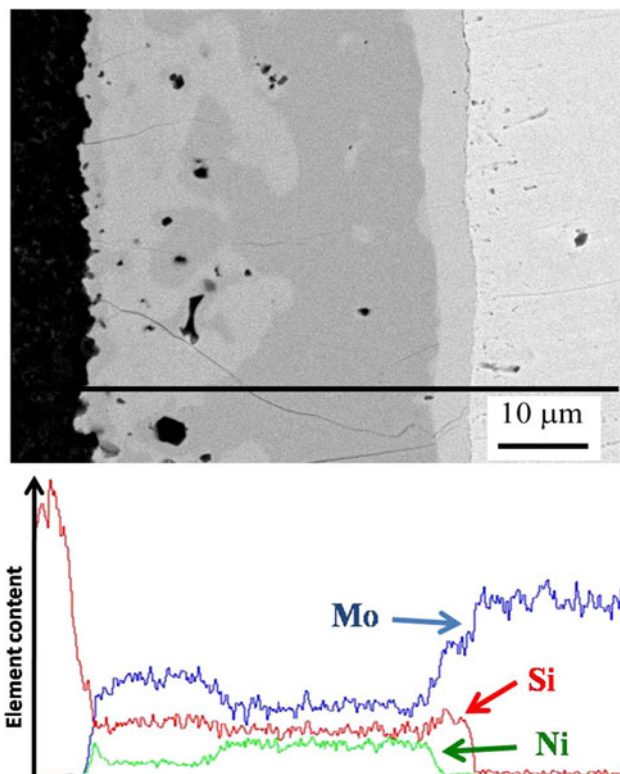
Fig. 4 EDS profiles across the SiC/Mo interface of a SiC/SiC joint prepared by Process A under the conditions of 1,350 °C × 10 min, showing the elemental diffusion along the *black line* in the micrograph

Figure 6 shows the fracture surfaces of two joints prepared by the two joining processes under the same conditions of 1,350 °C × 10 min. Going from the SiC body to the Mo, different layers are found, namely a very thin C layer (SiC–C interface), a Mo–Ni–Si–C (C/Ni–Si–Mo interface) and the Ni–Si–Mo layer adjacent to the Mo foil (Fig. 6b). Therefore, the fracture path passes along the SiC

body, the carbon layer, the C/Ni–Si interface and Ni–Si layer in turn, as shown in Fig. 7.

Reference can be made to Fig. 2 to explain the presence of the carbon layer at the SiC surface. Indeed, in the ternary Ni–Si–C system, when the Si activity decreases from its original value in the Ni–56Si liquid alloy, the system enters the zone where C can nucleate in the liquid phase and precipitate out of it, preferably at the liquid/SiC interface. When Mo is added to the system, as shown in Fig. 4, the situation is no longer the same and should be interpreted with the aid of the quaternary phase diagram, which is not yet available. However, starting from the available ternary diagrams C–Mo–Si [46], C–Mo–Ni [46], C–Ni–Si (Fig. 2), and Mo–Ni–Si [47], a tentative quaternary diagram can be inferred, which suggests that Mo additions to the C–Ni–Si system enlarge the domain of stability of the liquid phase with pure (solid) C. The analysis of elements across the interface shows that Mo dissolves into the Ni–Si alloy and forms a richer phase close to SiC. The experimental fact that carbon segregates seems to confirm that, as already said, Mo entering into the liquid phase depresses the C solubility by lowering the Si activity, which is similar to what happens in the Ni–Si–C ternary system.

Moreover, a large amount of Mo diffuses into the bulk Ni–Si coating, resulting in a sharp increase of surface tension of the liquid phase due to the high surface tension of Mo [48]. As in the previous study, the Ni–Si/Mo system [28] has shown that in the temperature range 1,200–1,350 °C, the spreading rate is very fast with a final contact angle is close to 0°, the bonding between SiC and the interlayer gets stronger according to the work of adhesion calculated by the Young–Dupré equation ($W_a = \sigma_{LV} (1 + \cos\theta)$).

The joints prepared by Process B at 1,350 °C fracture mainly in the SiC near the interface (Fig. 6c). However, the ruptures of other joints, prepared by this process at 1,375 and 1,400 °C, occur at the SiC level (Table 2).

Fig. 5 SiC/SiC joint (**a**), test specimens cut for the shear test (**b**), and scheme of the shear test fixture (**c**)
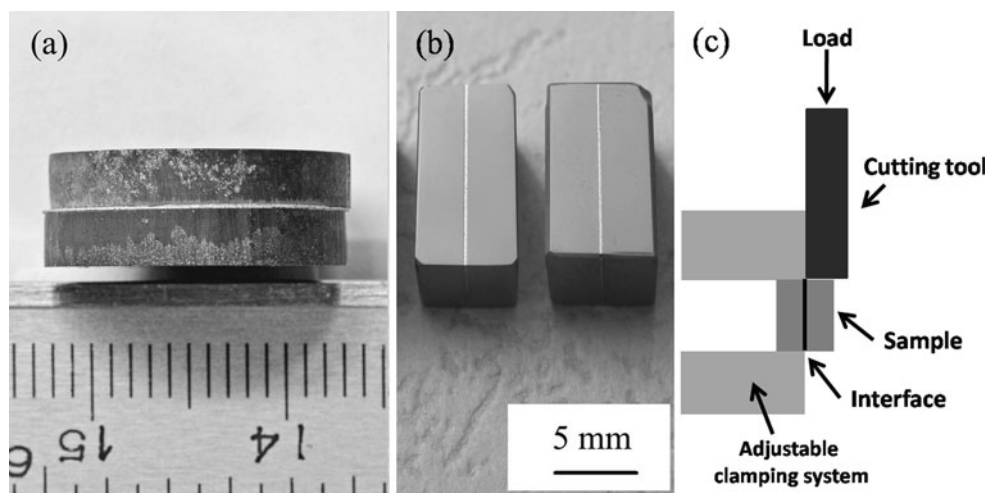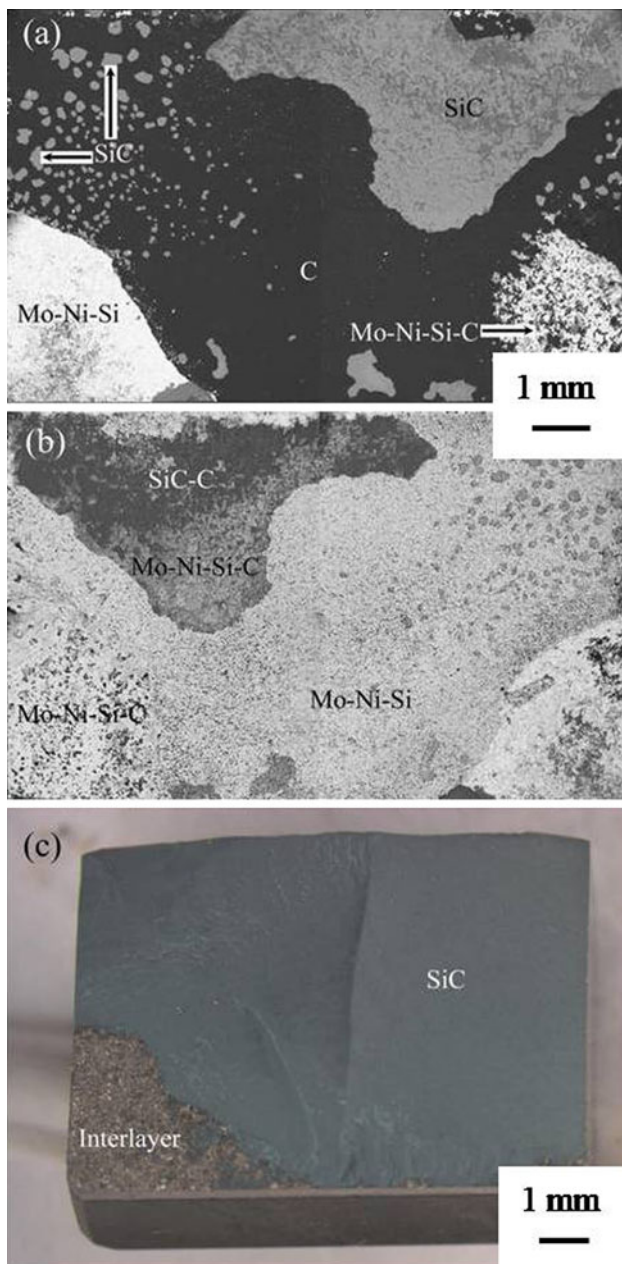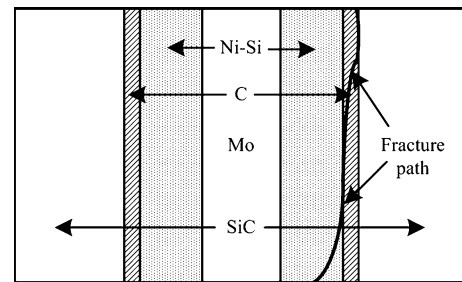
Table 2 Shear strength and fracture characteristics of joints prepared by the two processes

Joining process	Conditions	Shear strength (MPa)	Fracture zone
A (with pre-wetting)	1,350 °C × 10 min	27	Fracture in the interlayer
A	1,350 °C × 30 min	11	Fracture in the interlayer
A	1,350 °C × 50 min	10	Fracture in the interlayer
B (without pre-wetting)	1,350 °C × 10 min	41	Fracture in the SiC near the interface
B	1,375 °C × 10 min	–	Fracture at the SiC level
B	1,400 °C × 10 min	–	Fracture at the SiC level

Fig. 6 Fracture surfaces of two joints prepared under the same conditions of 1,350 °C × 10 min: **a** and **b** two sides of the same specimen prepared by the Process A (SEM-BS images); **c** the side with Mo in Process B

Fig. 7 Sketch of fracture path of joints prepared by Process B

To summarize, Process B is better, considering the joint strength value and the technological simplicity.

The strength of the joints obtained at longer holding times is low and the fracture occurred between layers E and F as indicated in Fig. 3c. However, layer F seems to adhere strongly to the SiC substrate.

Mo/Kovar bonding

Figure 8 shows the SEM micrographs of two cross-sectioned Mo/Kovar joints prepared by transient liquid phase bonding. An interfacial layer (~ 15 μm) with the composition Fe: 29%, Co: 9%, Ni: 14%, and Mo: 48%, forms near the Mo component. Element profiles obtained by EDS analysis, show that Mo diffuses a long way into the Kovar component, forming a wide diffusion zone, while Kovar constituting elements do not penetrate into the molybdenum. Increasing the holding time leads to an evolution of the microstructure with the formation of a large eutectic layer between the interfacial layer and the Kovar component (Fig. 8b). The gray and dark phases in this layer are Mo-rich and Fe-rich phases, respectively.

Differential thermal analysis tests performed up to 1,350 °C on the Mo–Kovar couple revealed (Fig. 9) an endothermic peak occurring at 1,303 °C and a mild endothermic process at 1,336 °C during heating. Both these processes disappeared during the cooling ramp. Moreover, a meniscus was found after tests at the corner between the two materials (Fig. 10), confirming that, during heating of the two components in contact each other, a liquid phase is formed at the interface below the melting points of both
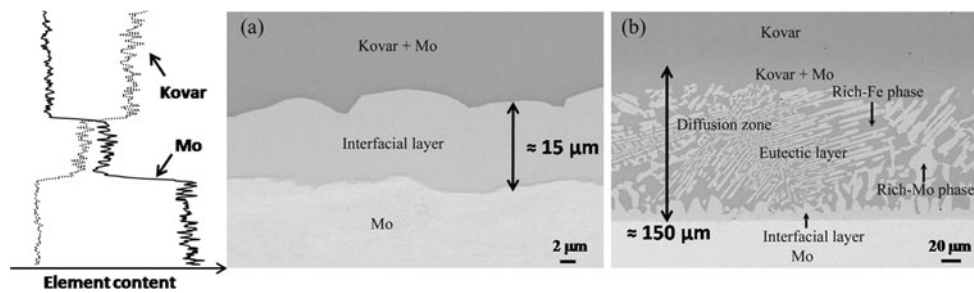
Fig. 8 SEM micrographs (BS mode) of two cross-sectioned Mo/Kovar joints prepared by diffusion bonding at 1,350 °C for different holding times: **a** 10 min and **b** 20 min. On the left: content profile along the A–B line, of Mo and Kovar constituting elements for the 10 min test
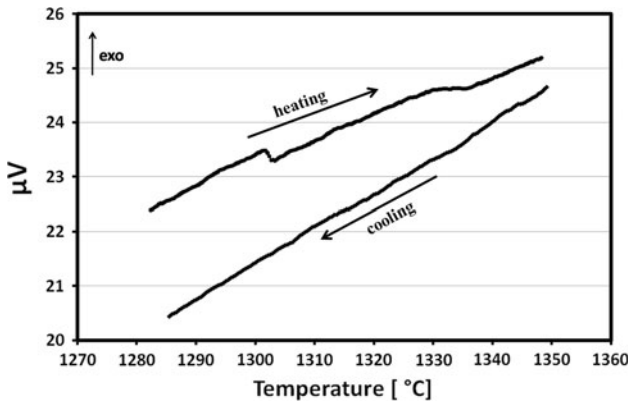

Fig. 9 Plots of DTA conducted on a Mo/Kovar couple (*x*-axis: temperature, *y*-axis: difference between the thermocouples signals of sample and reference)
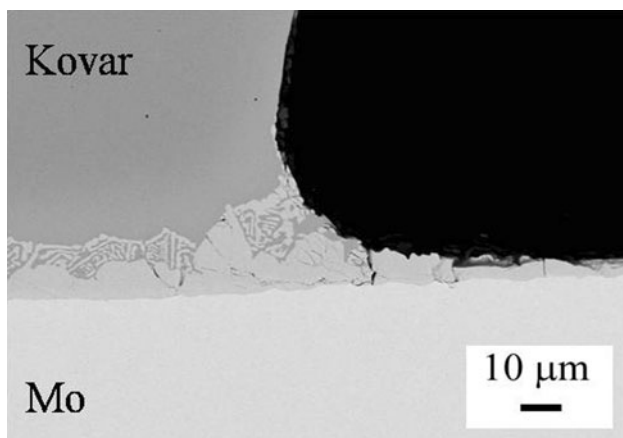

Fig. 10 SEM micrograph (BS mode) of a cross-sectioned Mo/Kovar joint showing the meniscus formed at the Mo–Kovar corner

Mo (2,617 °C) and Kovar (1,450 °C). The amount of this liquid phase is supposed to be very low; it solidifies afterward, during the holding time forming, by diffusion, the structures shown in Fig. 8. The isothermal solidification process is certified by the absence of any exothermic peak in the cooling curve.

SiC/Kovar joining

Figure 11 shows the SEM micrographs of a cross-sectioned SiC/Kovar joint obtained by using a SiC/Ni–Si/Mo/Kovar multilayer structure and coupling the two processes described before. The compositions of characteristic microstructures in the joint are listed in Table 3. As expected, a macroscopically smooth and clean SiC/interlayer interface forms without any observable reaction products with the ceramic component. Similarly to what was described in the previous sections, some interfacial layers grow at the Kovar/Mo and the Mo/Ni–Si interfaces, due to strong interactions (Fig. 11b, c). Moreover, in the filler layer, traces of the Kovar constituting elements were found (zones D and F) together with a small quantity of dark phases, with a high content of Ni, the presence of Fe and Co and without Mo, which are embedded in the gray phases, as shown in Fig. 11c and Table 3. The presence in this region of Fe and Co from the Kovar is justified by lateral capillary infiltration into the SiC/Ni–Si interface of the liquid phase formed at the Kovar/Mo interface.

Conclusions

A high-temperature method of brazing SiC to SiC was developed on the basis of wetting experiments of Ni–56 at.% Si alloy on SiC ceramic performed by the sessile drop technique at 1,350 °C in vacuum that confirmed the good, non-reactive wetting characteristics in the Ni–56Si/SiC system with an equilibrium contact angle of about 23°.

The SiC/SiC joints were fabricated by two joining processes using Ni–Si and Mo interlayers. Joint morphology, joint strength, and their fracture behavior were analyzed and discussed. A double-layer structure forms at all the Ni–Si/Mo interfaces due to strong interfacial interactions.

SiC is joined to Kovar by using a Ni–Si coating and Mo as interlayers on the SiC side, while the Mo is directly bonded to the Kovar. The Mo/Kovar joint is directly joined
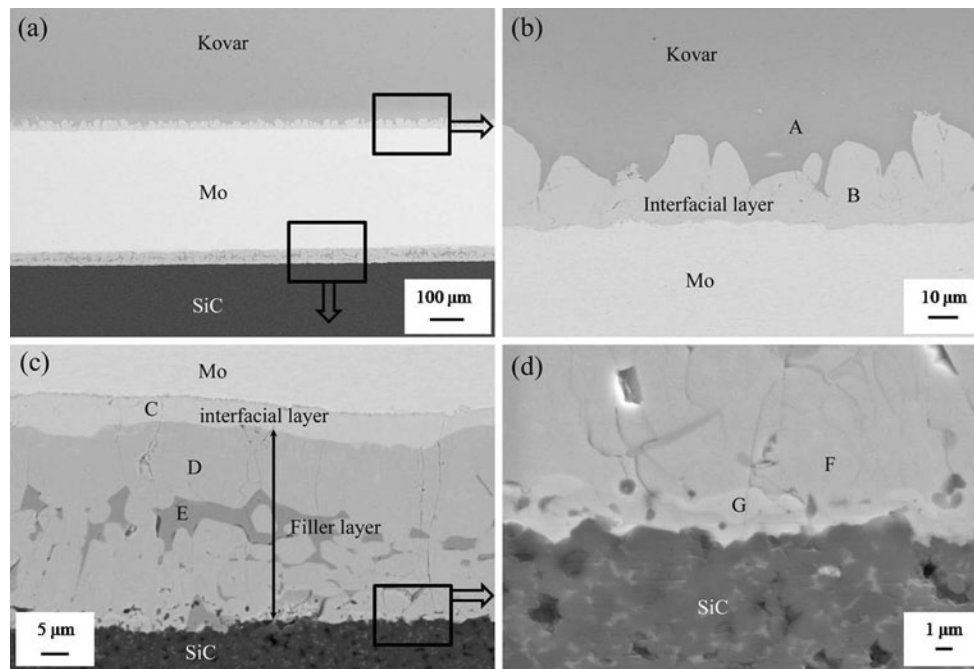
Fig. 11 SEM micrograps of a cross-sectioned SiC/Kovar joint: **a** Kovar/SiC joint; **b** Kovar/Mo interface; **c** Mo/Ni–Si/SiC section, and **d** Ni–Si/SiC interface

Table 3 Compositions of characteristic microstructures in the SiC/Kovar joint in Fig. 11

Position	Composition (at.%)				
	Fe	Ni	Co	Mo	Si
A	45.4	31.0	11.2	12.4	–
B	28.7	14.0	8.5	47.5	1.3
C	–	1.5	–	63.1	35.4
D	4.1	23.2	1.7	36.9	34.1
E	10.9	49.3	3.3	–	36.5
F	2.1	21.2	0.6	38.9	37.2
G	–	16.7	–	51.0	34.3

by means of the transient liquid phase bonding technique; the presence of a transient liquid phase, which evolves by diffusion, is confirmed by DTA analysis.

The joint interfacial morphologies, analyzed by SEM and EDS, show that two interfacial layers form at the Kovar/Mo and Mo/Ni–Si interfaces due to dissolution and interdiffusion phenomena between the metallic elements.

The type of joining process and the experimental conditions used, in particular the holding time, play a key role in determining joint microstructure and composition, joint strength, and their fracture behavior. This joining method is promising for joining SiC to alloys in high-temperature applications according to the joint microstructures. Further research on SiC/superalloy joining, in terms of joining technology and joint performances, are currently under way.

References

1. Jones RH, Giancarli L, Hasegawa A, Katoh Y, Kohyama A, Riccardi B, Snead LL, Weber WJ (2002) J Nucl Mater 307:1057
2. Katoh Y, Snead LL, Henager CH, Hasegawa A, Kohyama A, Riccardi B, Hegeman H (2007) J Nucl Mater 367:659
3. Steen M, Ranzani L (2000) Ceram Int 26:849
4. Xiong HP, Mao W, Xie YH, Chen B, Guo WL, Li XH, Cheng YY (2007) J Mater Res 22:2727
5. Xiong HP, Mao W, Xie YH, Chen B, Guo WL, Li XH, Cheng YY (2007) Mater Lett 61:4662
6. Chen B, Xiong HP, Mao W, Guo WL, Cheng YY, Li XH (2007) Acta Metall Sin 43(11):1181
7. Mao W, Li SJ, Han WB (2006) Rare Metal Mater Eng 35:312
8. Prakash P, Mohandas T, Raju PD (2005) Scr Mater 52:1169
9. Mcdermid JR, Drew RAL (1990) J Mater Sci 25:4804. doi: 10.1007/BF01129945
10. Mao YW, Li SJ, Yan LS (2008) Mater Sci Eng A 491:304
11. Cockeram BV (2005) J Am Ceram Soc 88:1892–1899
12. Liu HJ, Feng JC, Fujii H, Nogi K (2004) Mater Sci Technol 20:1069
13. Larker R, Nissen A, Pejryd L, Loberg B (1992) Acta metall Mater 40:3129
14. Yamada T, Satoh M, Kohno A, Yokoi K (1991) J Mater Sci 26:2887. doi:10.1007/BF01124817
15. Li SJ, Duan HP, Liu S, Zhang YG, Dang ZJ, Zhang Y, Wu CG (2000) Int J Refract Met Hard Mater 18:33
16. Li SJ, Zhou Y, Duan HP, Qiu JH, Zhang Y (2003) J Mater Sci 38:4065. doi:10.1023/A:1026135220737
17. Iino Y (1991) J Mater Sci Lett 10:104
18. Zhang CG, Qiao GJ, Jin ZH (2002) J Eur Ceram Soc 22:2181
19. Lemoine P, Ferraris M, Salvo M, Appendino Montorsi M (1999) J Eur Ceram Soc 16:1231
20. Mcdermid JR, Drew RAL (1991) J Am Ceram Soc 74:1855

21. Koltsov A, Hodaj F, Eustathopoulos N (2008) Mater Sci Eng A 495:259
22. Riccardi B, Nannetti CA, Woltersdorf J, Pippel E, Petrisor T (2004) Int J Mater Product Technol 20:440
23. Riccardi B, Nannetti CA, Woltersdorf J, Pippel E, Petrisor T (2002) J Mater Sci 37:5029. doi:10.1023/A:1021087632155
24. Tsoga A, Ladas S, Nikolopoulos P (1997) Acta Mater 45:3515
25. Tanaka SI, Iwamoto C (2008) Mater Sci Eng A 495:168
26. Laurent V, Rado C, Eustathopoulos N (1996) Mater Sci Eng A 205:1
27. Xiong HP, Li XH, Mao W, Cheng YY (2003) Mater Lett 57:3417
28. Liu GW, Valenza F, Muolo ML, Qiao GJ, Passerone A (2009) J Mater Sci 44:5990. doi:10.1007/s10853-009-3858-0
29. Rado C, Kalogeropoulou S, Eustathopoulos N (1999) Acta Mater 47:461
30. Mailliart O, Hodaj F, Chaumat V, Eustathopoulos N (2008) Mater Sci Eng A 495:174
31. Naidich YV, Zhuravlev V, Krasovskaya N (1998) Mater Sci Eng A 245:293
32. Rado C, Kalogeropoulou S, Eustathopoulos N (2000) Mater Sci Eng A 276:195
33. Rado C, Eustathopoulos N (2004) Interface Sci 12:85
34. Riccardi B, Nannetti CA, Petrisor T, Woltersdorf J, Pippel E, Libera S, Pillonni L (2004) J Nucl Mater 329:562
35. Riccardi B, Nannetti CA, Petrisor T, Sacchetti M (2002) J Nucl Mater 307:1237
36. Li JK, Liu L, Wu YT, Zhang WL, Hu WB (2008) Mater Lett 62:3135
37. Hattali ML, Valette S, Ropital F, Stremsdoerfer G, Mesrati N, Tréheux D (2009) J Eur Ceram Soc 29:813
38. Jin HY, Ishiyama M, Qiao GJ, Gao JQ, Jin ZH (2008) Mater Sci Eng A 483:270
39. Liggieri L, Passerone A (1989) High Temp Technol 7:82
40. Passerone A, Ricci E (1998) In: Möbius D, Miller R (eds) Drops and bubbles in interfacial research. Elsevier, Amsterdam, pp 475–524
41. Eustathopoulos N, Sobczak N, Passerone A, Nogi K (2005) J Mater Sci 40:2271. doi:10.1007/s10853-005-1945-4
42. Valenza F, Muolo ML, Passerone A (2010) J Mater Sci 45:2071. doi:10.1007/s10853-009-3801-4
43. Liu GW, Qiao GJ, Wang HJ, Yang JF, Lu TJ (2008) J Eur Ceram Soc 28:2701
44. Rado C, Kalogeropoulou S, Eustathopoulos N (1999) Acta Mater 47:461
45. Du Y, Schuster JC (1999) Metall Mater Trans 30:2409
46. Villars P, Price A, Okamoto H (1995) Handbook of ternary alloy phase diagram. ASM International, Materials Park
47. Gupta KP (2005) J Phase Equilib Diffus 26(4):379
48. Eustathopoulos N, Drevet B, Ricci E (1998) J Cryst Growth 191:268